Electronic Supplementary Information for

A ROS Storm Generating Nanocomposite for Enhanced Chemodynamic Therapy *via* H_2O_2 Self-Supply, GSH Depletion and Calcium Overload

Yong Li[a], Jing Wang[a], Tao Zhu[a], Ying Zhan[b], Xiaoli Tang[a], Jianying Xi[a], Xiaohui Zhu[a], Yong Zhang[c*] and Jinliang Liu[a*]

[a] School of Environmental and Chemical Engineering, Shanghai University, Shanghai, China, 200444.

[b] School of Life Science, Shanghai University, Shanghai, China, 200444.

[c] Department of Biomedical Engineering, City University of Hong Kong, 83 Tat Chee Avenue, Kowloon, Hong Kong.

yozhang@cityu.edu.hk (Yong Zhang) and liujl@shu.edu.cn (Jinliang Liu)

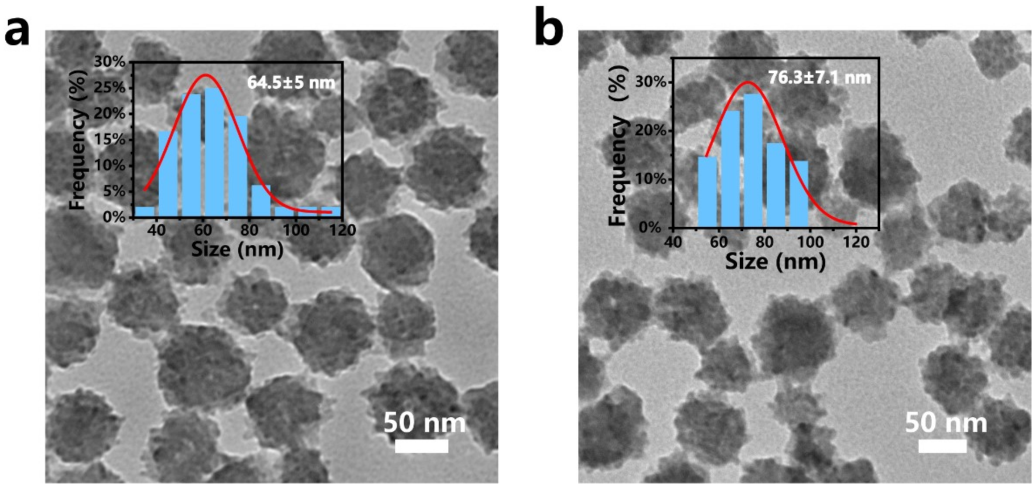

Figure S1. TEM images of (a) CaO_2 and (b) CaO_2@Cu. The CaO_2 nanoparticles feature a spheroidal morphology with well-defined size distribution of approximately 70 nm, the CaO_2@Cu NPs prepared exhibited enhanced dispersion, as evidenced by their average diameter of approximately 80 nm.

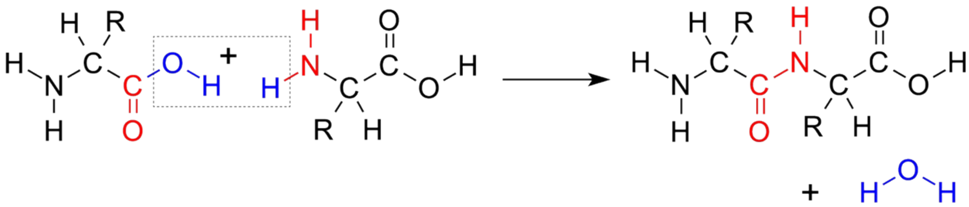

Figure S2. Dehydration condensation reaction between BSO molecules and CaO_2@Cu NPs.

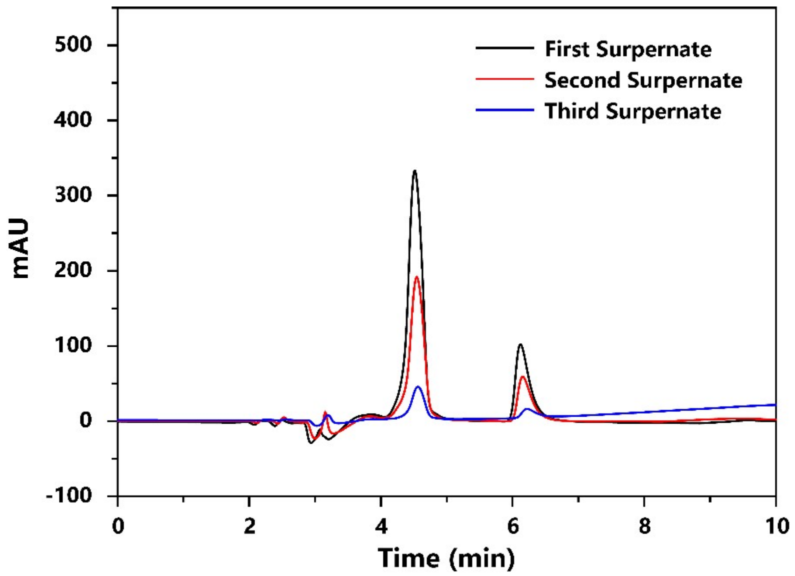

Figure S3. HPLC spectra of different samples.

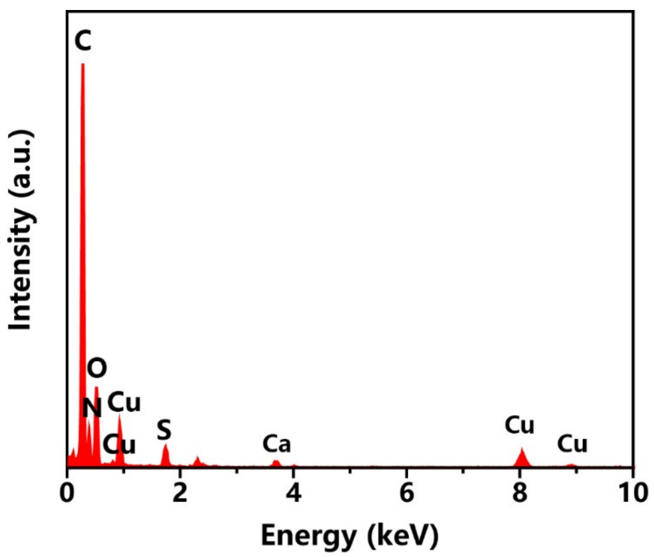

Figure S4. EDS spectrum of CaO_2@Cu-BSO NPs. Signals of N and S elements appeared in the elemental mapping, and EDS spectrum of CaO_2@Cu–BSO NPs showed the successful grafting of BSO molecules.

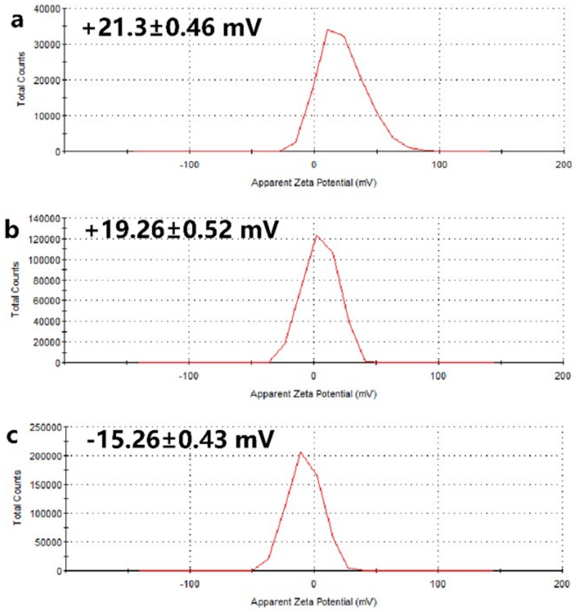

Figure S5. The apparent zeta potentials of (a) CaO_2, (b) CaO_2@Cu and (c) CaO_2@Cu-BSO. The surface zeta potentials of NPs changed from +21.3 to −15.26 mV after the introduction of negatively charged BSO grafted onto the particle surface.

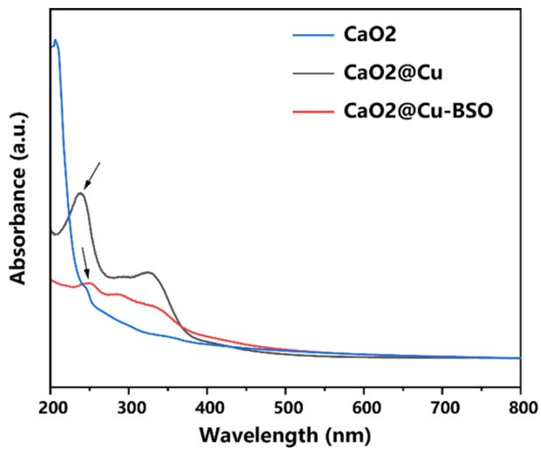

Figure S6. UV-vis spectra of CaO_2, CaO_2@Cu and CaO_2@Cu-BSO. CaO_2@Cu and CaO_2@Cu–BSO appear characteristic peaks at 239 nm and 252 nm in the UV-visible spectrum respectively.

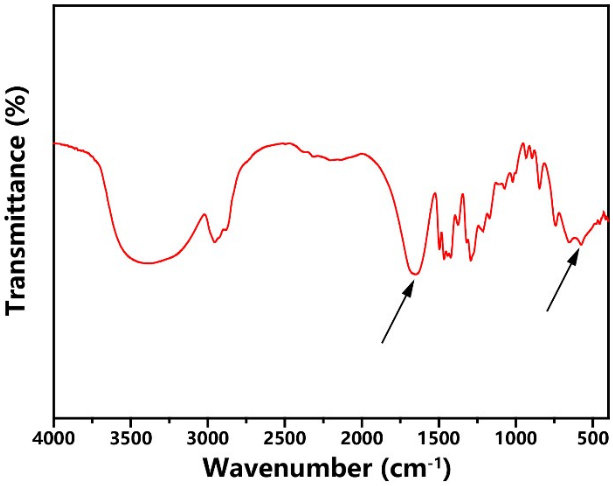

Figure S7. FT-IR spectra of CaO_2 nanospheres. The characteristic peak at 573.2 cm^{-1} is due to the O-Ca-O vibration. The absorption peak at about 1630.1 cm^{-1} is attributed to the stretching of the C = O bond, demonstrating the weak chemical coordination of PVP.

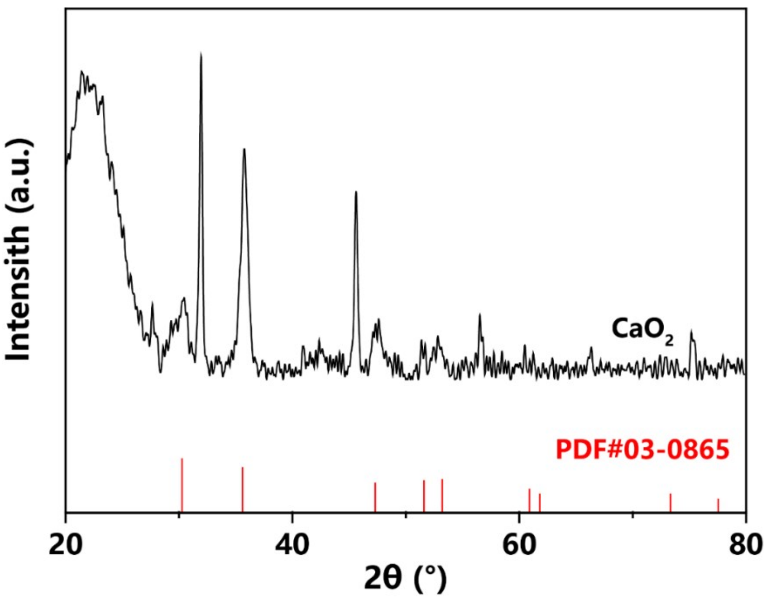

Figure S8. XRD patterns of CaO_2.

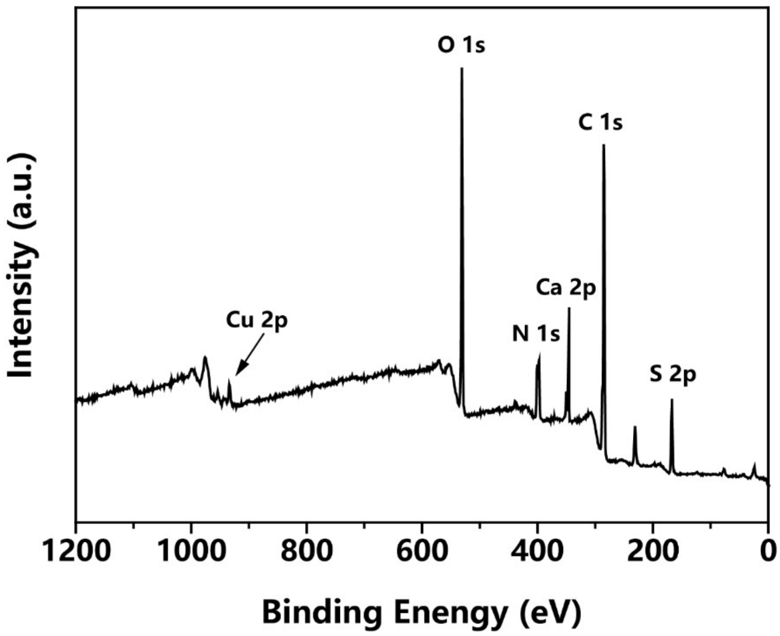

Figure S9. Full XPS spectrum of CaO_2@Cu–BSO NPs.

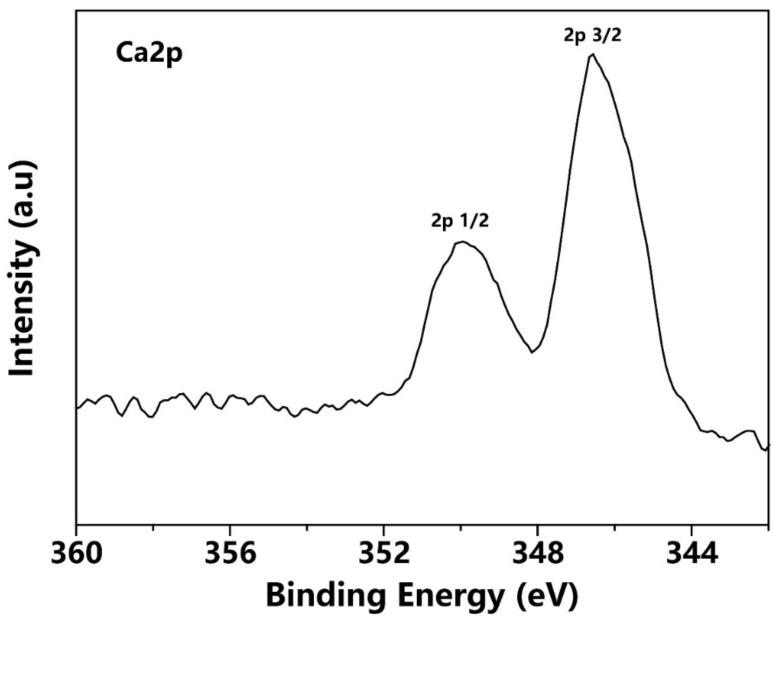

Figure S10. Ca 2p XPS spectrum of CaO_2.

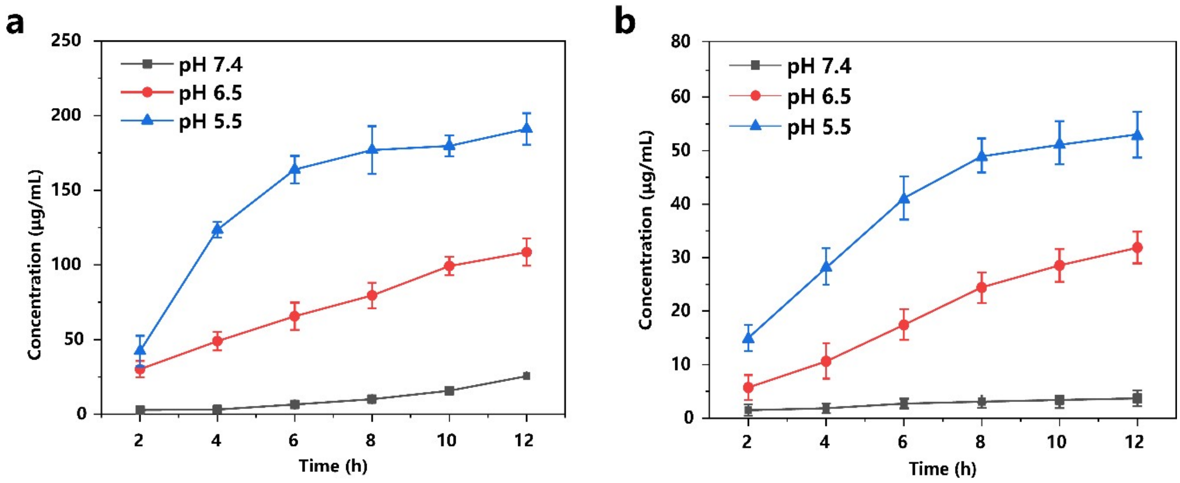

Figure S11. *In vitro* releases of (a) Ca^{2+} and (b) Cu^{2+} from CaO_2@Cu-BSO dispersed in solutions with different pH values (mean ± SD, n=3).

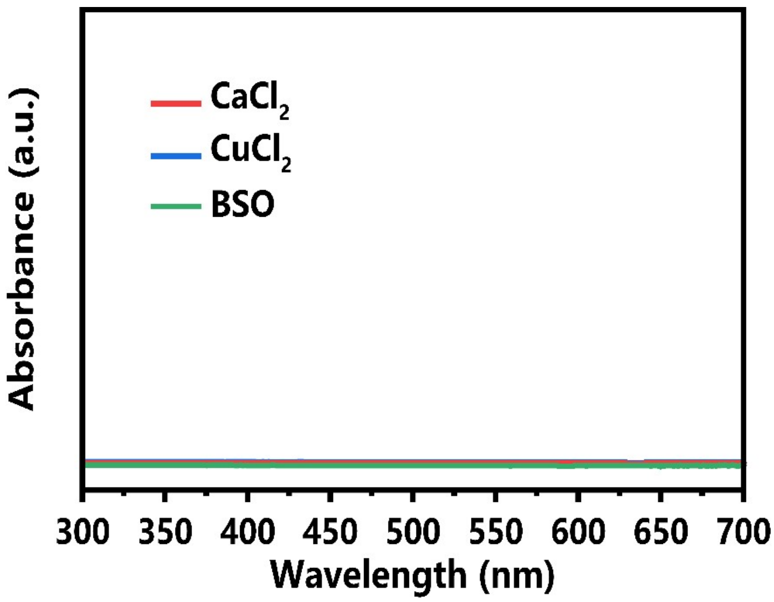

Figure S12. UV-vis absorbance spectra of $Ti(SO_4)_2$ solution in presence of $CaCl_2$, $CuCl_2$ and BSO (100 μg/mL for each agent).

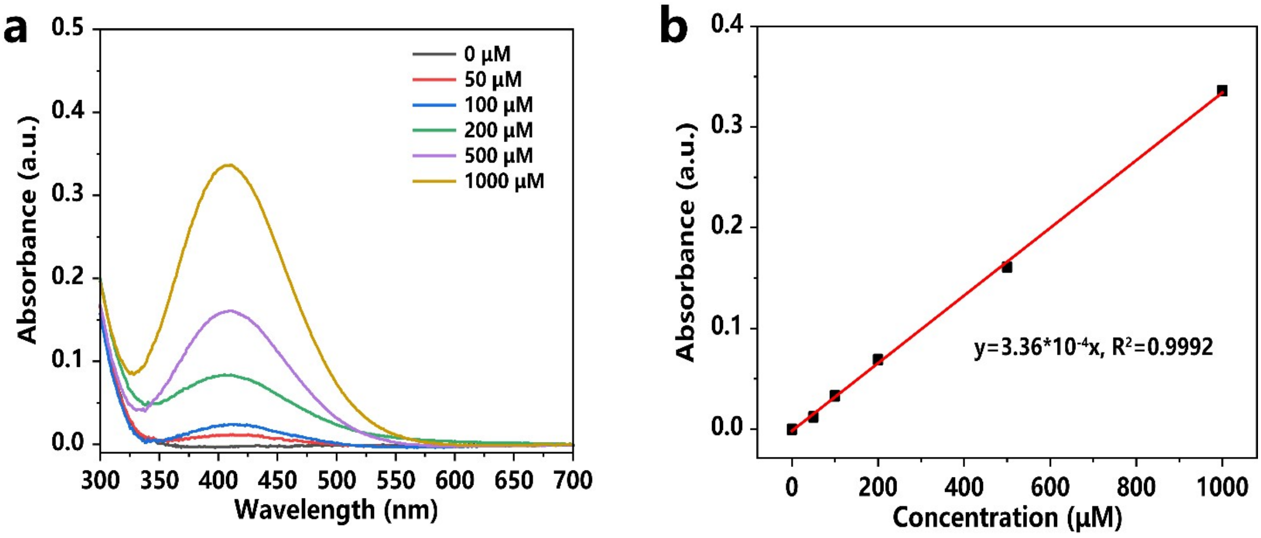

Figure S13. (a) UV–vis absorption spectra of $Ti(SO_4)_2$ solution mixed with various concentrations of H_2O_2. (b) Plot of absorbance versus concentrations of H_2O_2, based on the different absorbance at 410 nm wavelength.

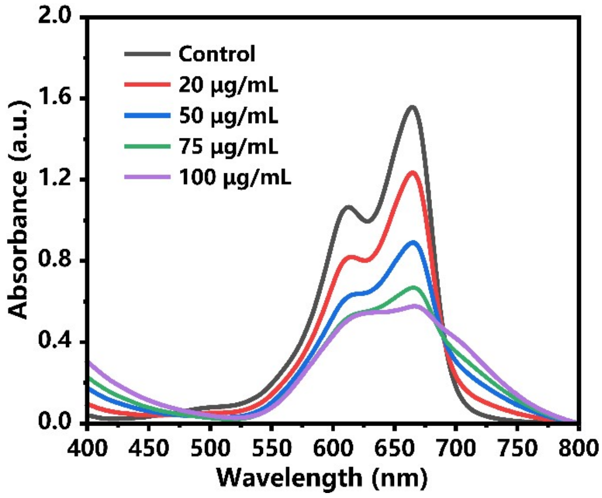

Figure S14. UV–Vis spectra of MB incubated with CaO_2@Cu–BSO NPs containing different concentrations.

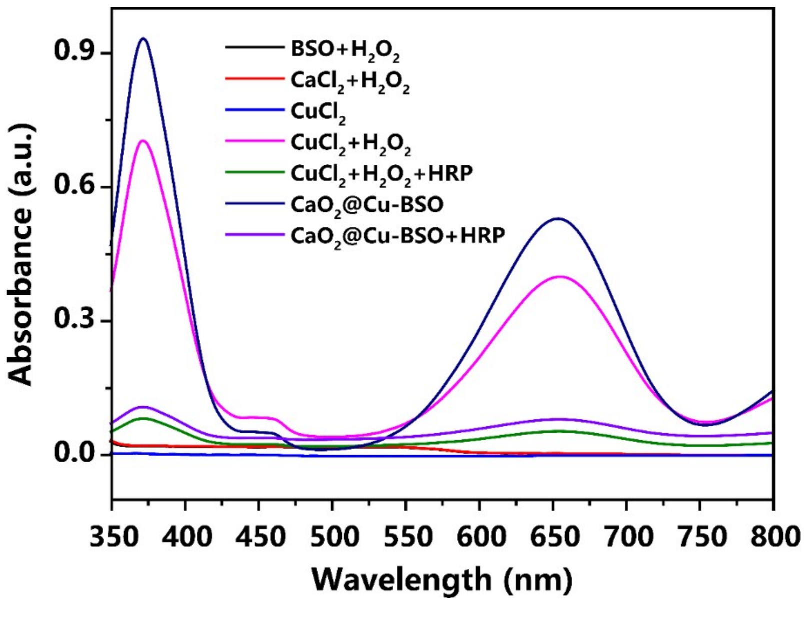

Figure S15. UV–vis absorbance spectra of ox-TMB in the presence of various samples.

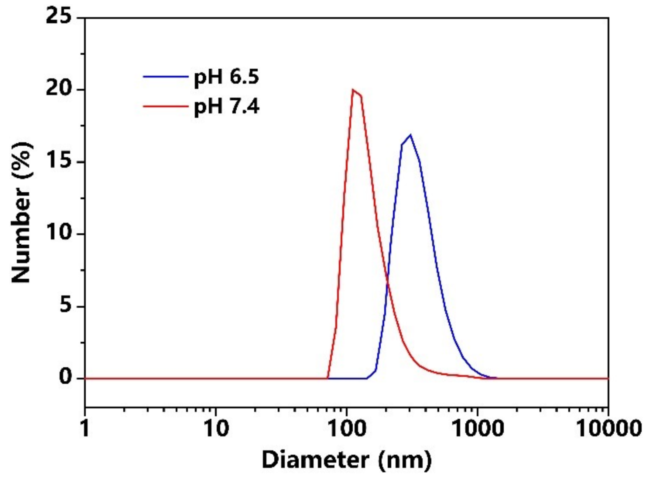

Figure S16. DLS results of CaO_2@Cu-BSO NPs incubated in 1640 media for 12 h under different pH.

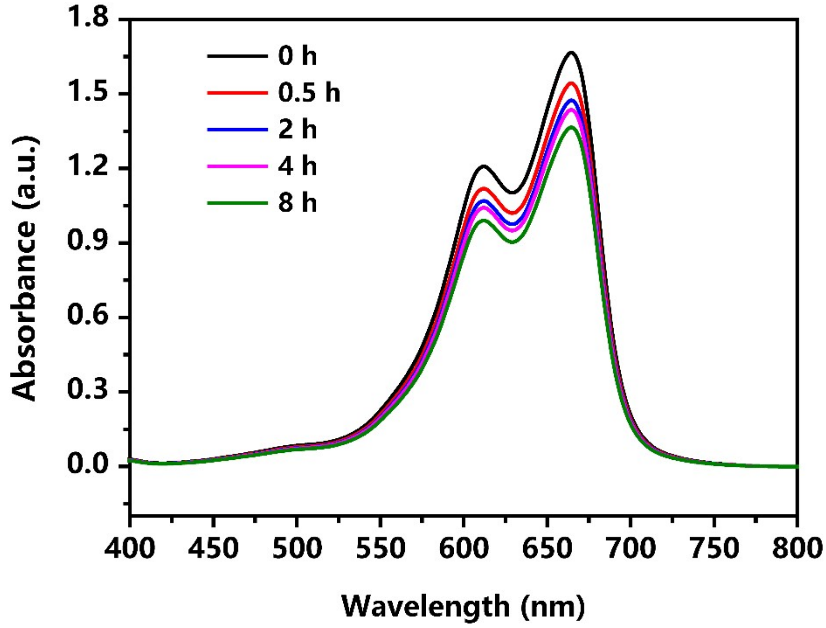

Figure S17. UV−Vis spectra of MB incubated with H_2O_2 under different time.

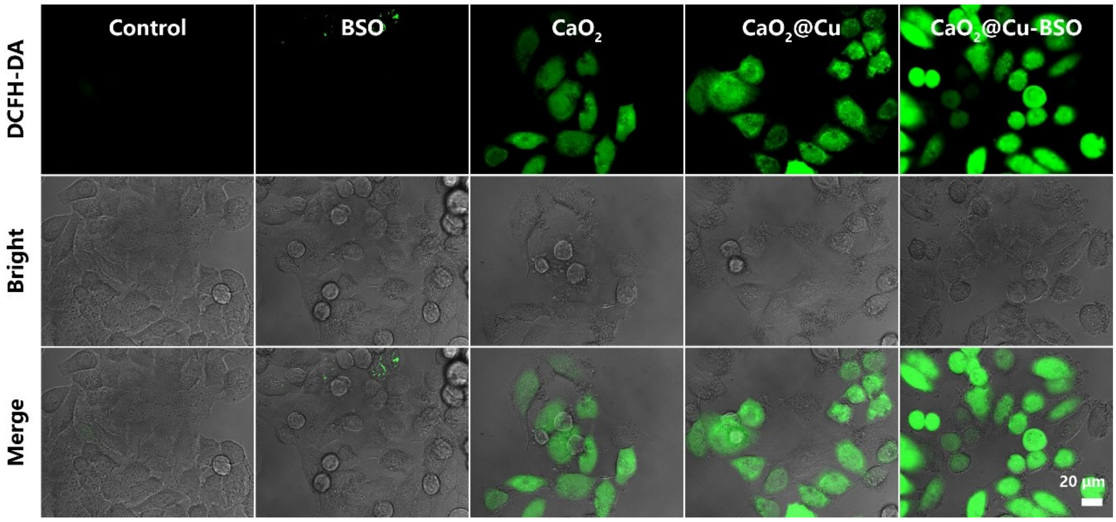

Figure S18. Fluorescence image of A549 cells incubated with BSO after DCFH-DA staining for ROS detection (CaO_2 concentration was unified at 50 μg/mL).

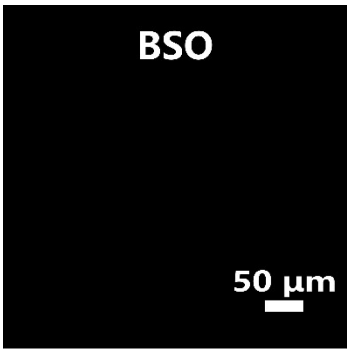

Figure S19. Fluorescence image of A549 cells incubated with BSO after DCFH-DA staining for ROS detection.

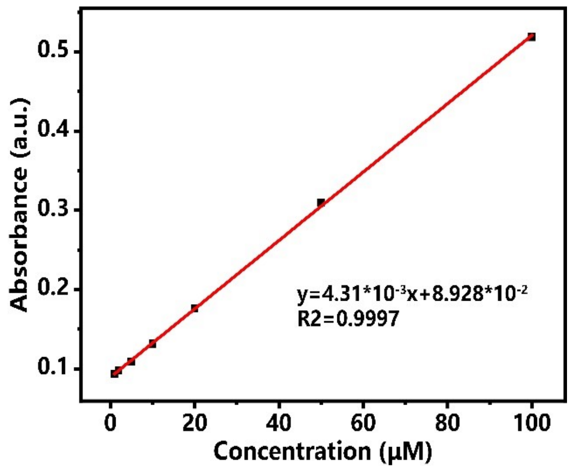

Figure S20. Plot of absorbance versus concentrations of H_2O_2, based on the H_2O_2 Kit.

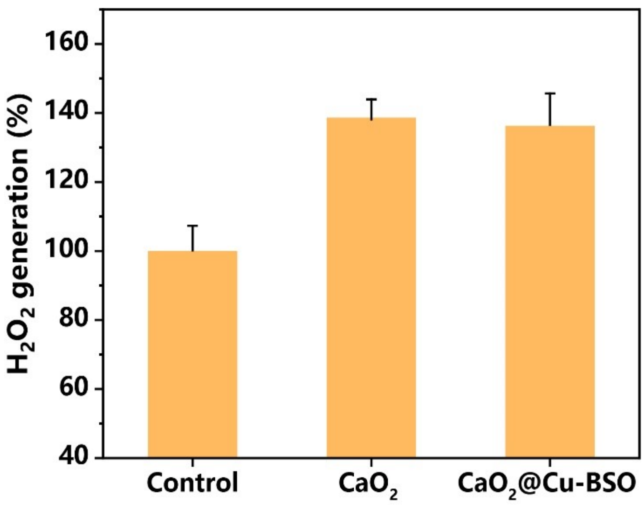

Figure S21. Comparison of intracellular H_2O_2 in A549 cells cultured with CaO_2@Cu-BSO NPs or CaO_2 NPs (CaO_2 concentration was unified at 50 μg/mL, mean ± SD, n = 3.).

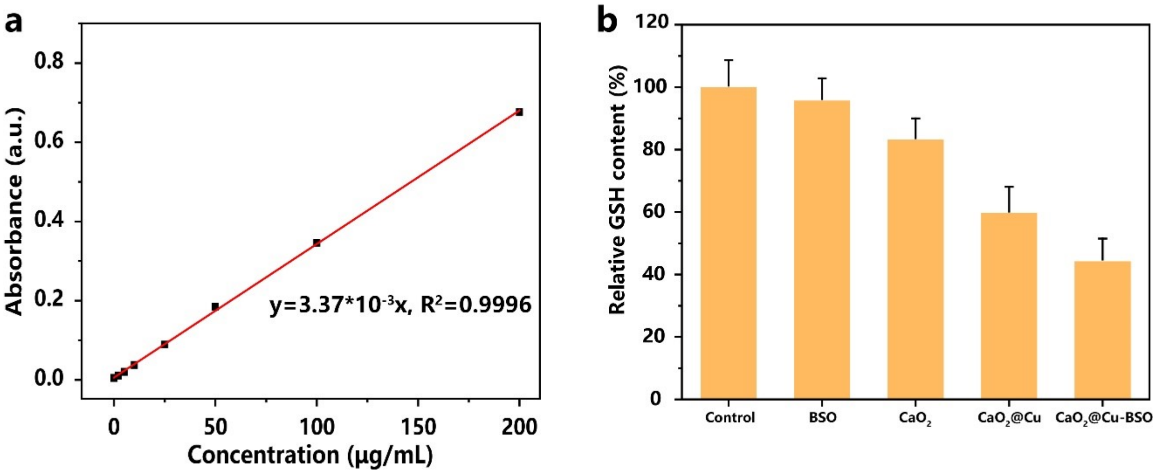

Figure S22. (a) Plot of absorbance versus concentrations of GSH, based on the GSH Kit. (b) Intracellular GSH level in A549 treated with different samples (CaO_2 concentration was unified at 50 μg/mL, mean ± SD, n = 3).

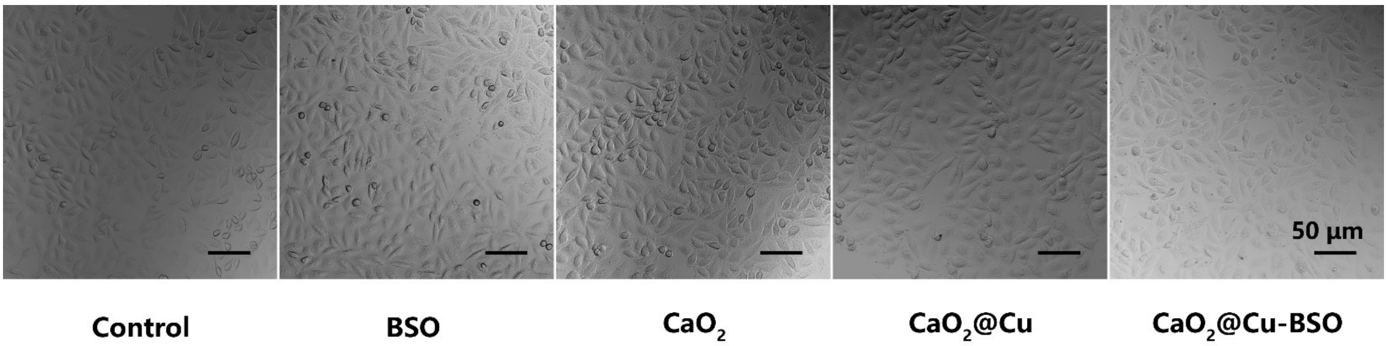

Figure S23. Bright field images of A549 cells incubated with different samples after NDA staining for GSH detection.

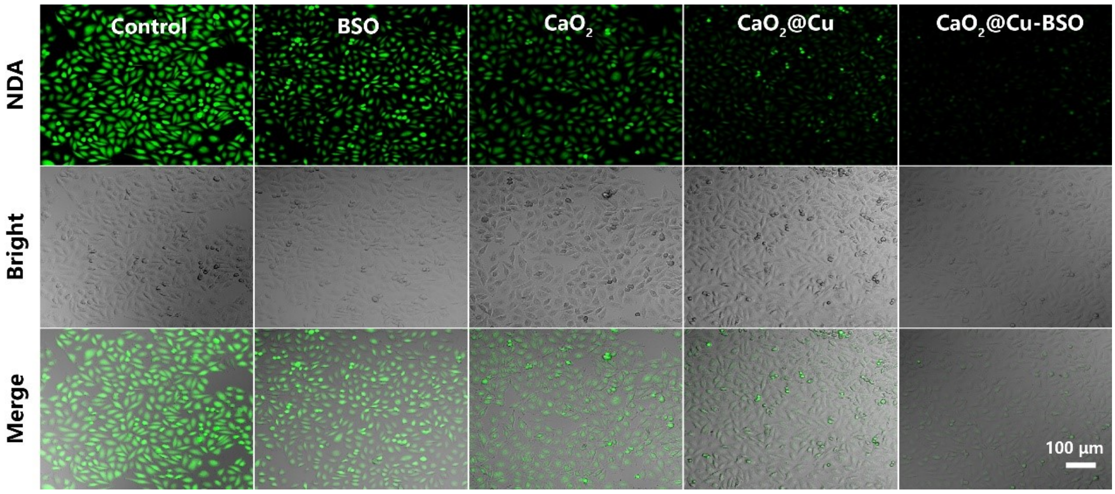

Figure S24. Images of A549 cells incubated with different samples after NDA staining for GSH detection (CaO_2 concentration was unified at 50 μg/mL).

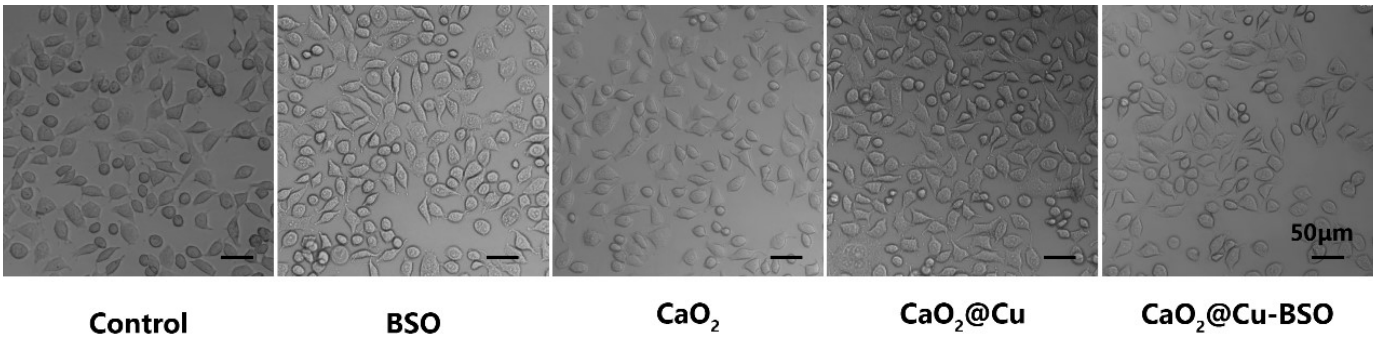

Figure S25. Bright field images of A549 cells incubated with different samples after Fluo-4 AM staining for intercellular Ca^{2+} accumulation.

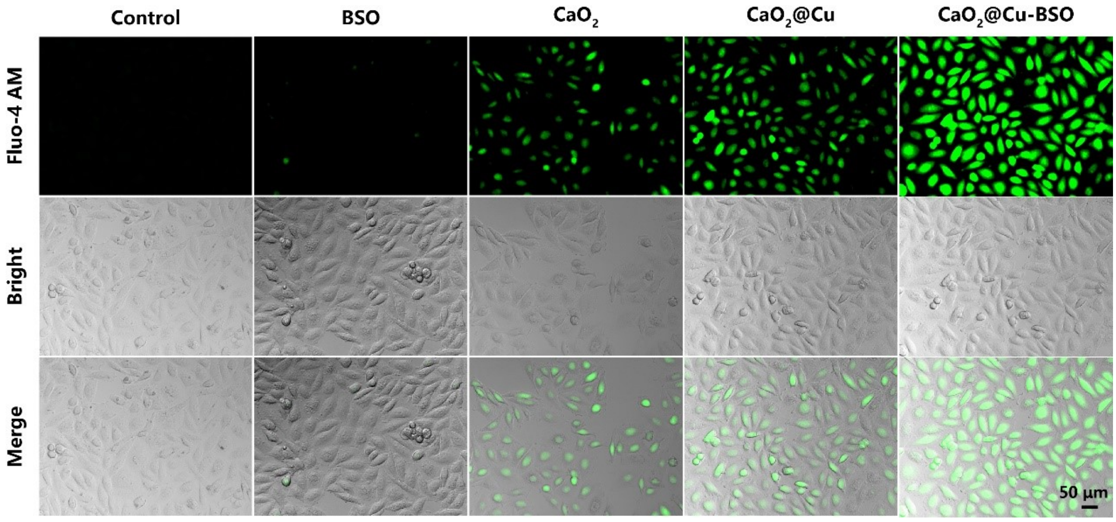

Figure S26. Images of A549 cells incubated with different samples after Fluo-4 AM staining for intercellular Ca^{2+} accumulation (CaO_2 concentration was unified at 50 μg/mL).

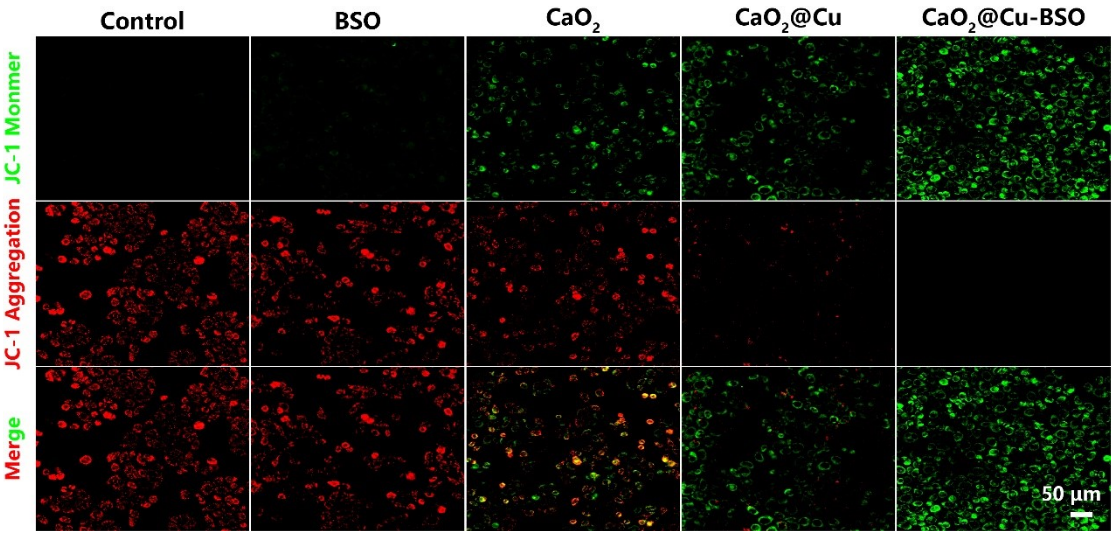

Figure S27. CLSM images of JC-1assays of A549 cells under different conditions (CaO_2 concentration was unified at 50 μg/mL).

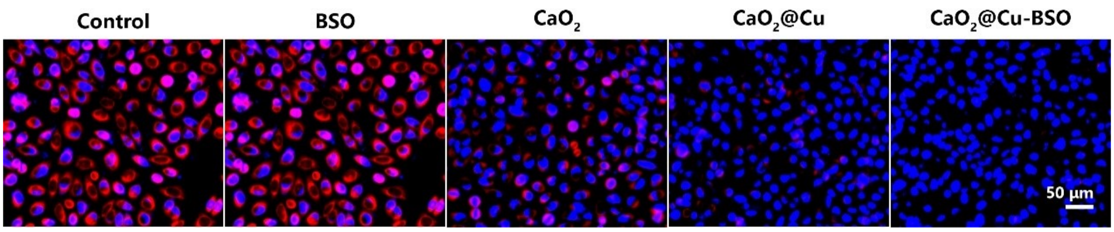

Figure S28. CLSM images of A549 cells treated with different samples and then stained with MitoTracker Red and Hoechst 33258 (CaO_2 concentration was unified at 50 μg/mL).

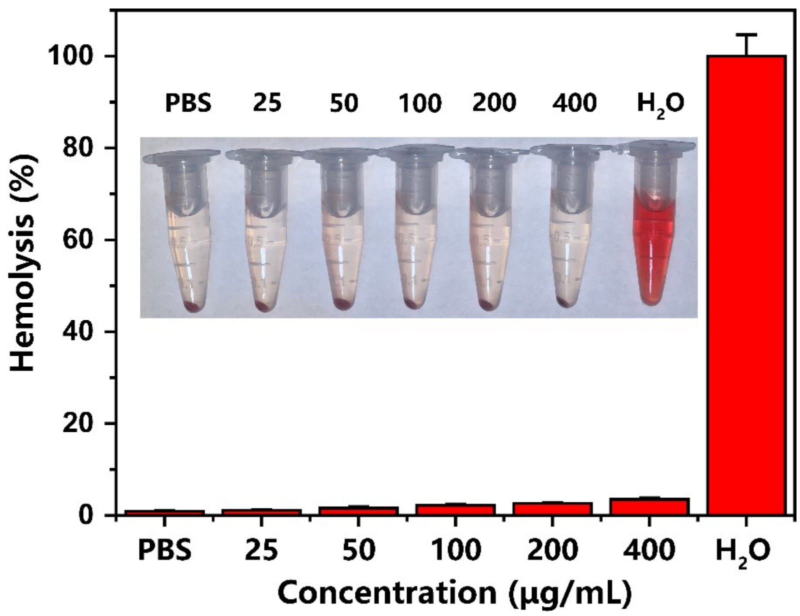

Figure S29. Hemolysis analysis of CaO_2@Cu-BSO NPs suspension at various concentrations (mean ± SD, n=3).

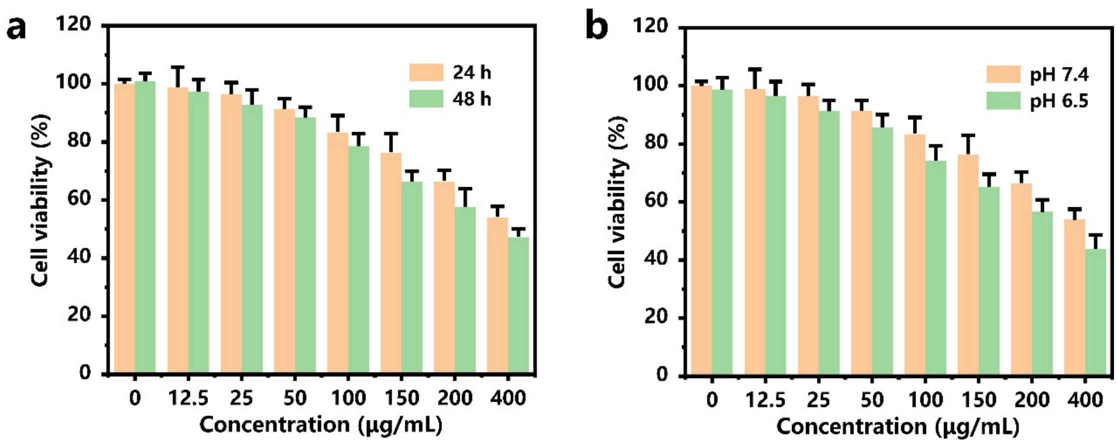

Figure S30. (a) Cell viabilities of A549 cells treated with different concentrations of CaO_2@BSO NPs for 24 and 48 h. (c) Cell viabilities of A549 cells treated with different concentrations of CaO_2@BSO NPs at pH 7.4 and pH 6.5 (mean ± SD, n=3).

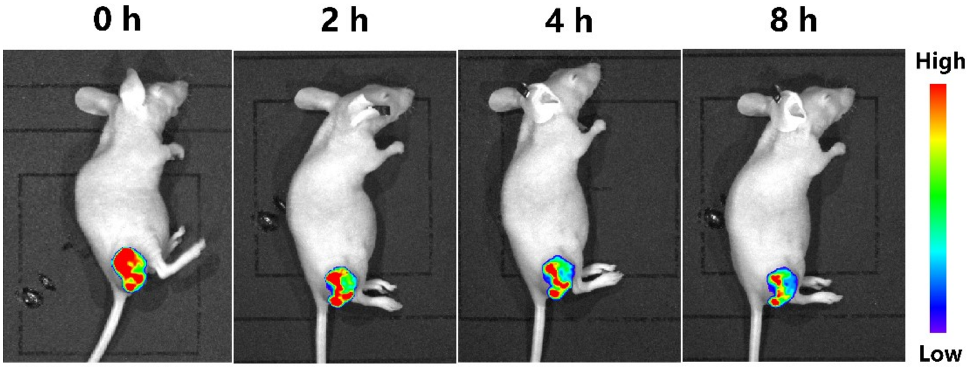

Figure S31. Fluorescence images of tumor–bearing mice after intratumoral injection with Rb labeled CaO_2@Cu-BSO NPs for different times.

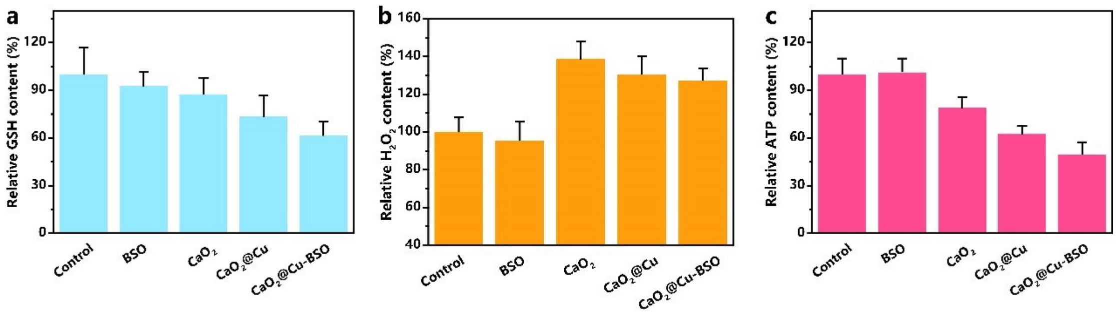

Figure S32. (a) GSH, (b) H_2O_2 and (c) ATP content determination of the tumor regions from different groups (mean ± s.d., n = 3).

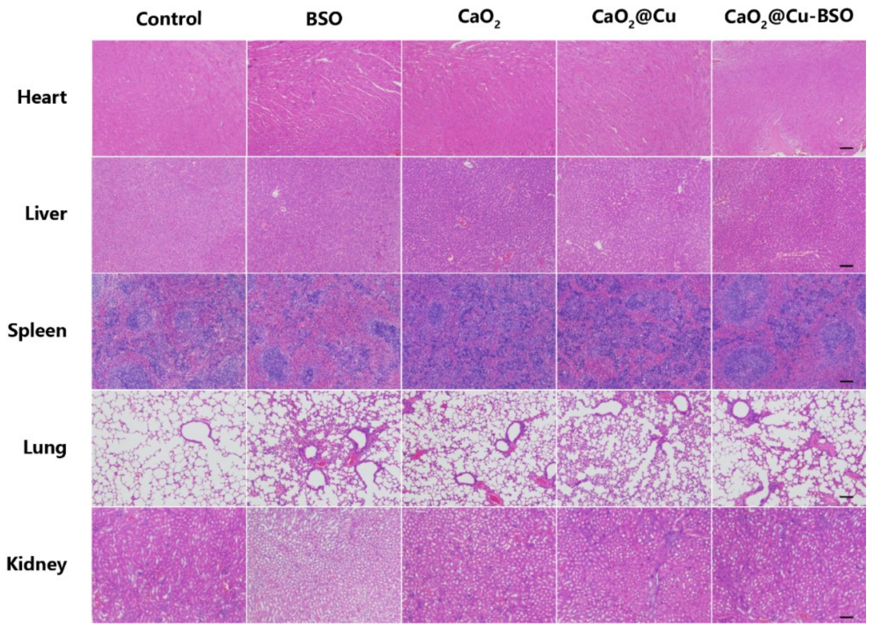

Figure S33. Histological analyses of tissues by hematoxylin and eosin (H&E) staining of major organs heart, liver, spleen, lung and kidney. Scale bar = 100 μm.